Molecular Mechanism of Solvent-Induced Crystallization of Syndiotactic Polystyrene Glass. 2. Detection of Enhanced Motion of the Amorphous Chains in the Induction Period of Crystallization

Kohji Tashiro* and Akiko Yoshioka

Department of Macromolecular Science, Graduate School of Science, Osaka University, Toyonaka, Osaka 560-0043, Japan

Received August 21, 2001; Revised Manuscript Received October 15, 2001

ABSTRACT: Syndiotactic polystyrene (sPS) glassy sample crystallizes into the polymer−solvent complex of δ form with T_2G_2 helical conformation when it is exposed to the atmosphere of organic solvent. This solvent-induced crystallization is observed at room temperature, much lower than the glass transition temperature of sPS. This experimental fact implied that the molecular motion of the amorphous chains should be enhanced more or less by absorption of solvent even below the glass transition temperature. This prediction could be confirmed experimentally by measuring the time-dependent change in the half-width and peak position of the infrared bands of the amorphous chains on the basis of such an idea that the half-width is larger and the vibrational frequency is lower as the molecular motion is accelerated to higher extent. In fact, the half-width was found to increase largely, and the peak position shifted toward lower frequency side when the solvent was supplied to the glassy sPS sample, indicating an enhancement of the amorphous chain motion by which the random coils were regularized to form short helical segments. As the time passed furthermore, the helical length was found to increase, and these long helices gathered together to form the crystalline lattice, as being observed in the remarkable increment of the crystalline peaks of the infrared and Raman bands as well as the X-ray diffraction intensity. The accelerating rate of molecular motion of the amorphous chain and the formation rate of regular helical chains were found to be dependent on the kind of solvent used in the experiment: chloroform, benzene, and toluene.

Introduction

Syndiotactic polystyrene (sPS) exhibits the various crystalline modifications depending on the sample preparation conditions.[1] Roughly speaking, random coils of the glassy state regularize to the planar zigzag conformation in the α (trigonal packing of chains) and β (orthorhombic packing of chains) crystalline forms by annealing the glass sample above the glass transition temperature (T_g)[2] or to the δ form by absorption of organic solvent where the polymer chains of $(T_2G_2)_2$ helical conformation form a complex with solvent molecules.[3] By heating the δ form above 120 °C, it transforms to the γ form with keeping the chain conformation of $(T_2G_2)_2$ type.[4] This γ form transfers to the α or β form by heat treatment at higher temperature.

In the previous papers,[5−7] we carried out the time-resolved measurements of infrared, Raman, and X-ray diffraction, from which the details of the structural regularization process could be described successfully from the viewpoints of molecular conformation and aggregation structure of the chains. At that time it was simply considered without any deep insight that the amorphous chains can regularize spontaneously into the helices by absorbing solvent. But the glass transition temperature (T_g) of sPS is about 100 °C, much higher than room temperature where the experiment was performed. In general, the crystallization of the amorphous chains is processed with heating the glassy sample above T_g so that the amorphous chains become more mobile. But, the solvent-induced crystallization of sPS sample can be induced at room temperature much lower than T_g. Therefore, we may speculate reasonably that the motion of the molecular chains in the amorphous region is accelerated when the chains interact with the solvent molecules. In other words, the solvent is speculated to play a role as a plasticizer to induce the crystallization of the amorphous phase. To prove this speculation experimentally, the molecular motion must be detected directly by any physicochemical method. This experimental proof of the chain motion in the amorphous region is quite important to understand the crystallization process of this polymer from the molecular level.

The purpose of the present paper is to collect the experimental data to support the above-mentioned hypothesis of the molecular motion of the amorphous chains in this solvent-induced crystallization phenomenon. We might have various methods for this purpose. The solid-state NMR method might be one of the possible candidates. But the induction period in the crystallization process is too short to be detected by this method. Besides, it is difficult to introduce the solvent into the rapidly spinning NMR sample tube. The measurement of dielectric dispersion spectra might be another candidate: the dielectric loss peak corresponding to the chain motion in the amorphous phase should be observed when the solvent is introduced into the sample. In this experiment the film surface must be contacted directly to the metal electrode, making an invasion of solvent vapor into the sample film difficult. This direct contact of the electrode is needed because of such a reason that the exact evaluation of the dielectric constant of the sample itself becomes very difficult when any small gap is present between the sample surface and the metal electrode, since the dielectric constant of solvent (and air) might be overwhelmingly larger than that of the sample. The dynamic viscoelastic measurement can be used, but the full filling of the solvent vapor in the large sample box is experimentally awful.

Then we got an idea to measure the change in the half-width of the infrared band intrinsic of the amor-

10.1021/ma011509x CCC: $22.00
Published on Web 12/14/2001

phous structure after the solvent vapor injection. This is based on such an idea that the half-width of an infrared band is a measure of the molecular motion, and it is inversely proportional to the relaxation time of the motion of the groups associated with this vibrational band.[8] The band is broader as the motion is more vigorous or the relaxation time is shorter: $\Delta\nu \propto 1/\tau$, where $\Delta\nu$ is a half-width of an IR band and τ is a relaxation time of the molecular motion associated with this vibrational band. To check the usefulness of this idea, we measured, as an example, the temperature dependence of the half-width of the infrared band of the amorphous atactic polystyrene (aPS) sample. Then we applied this idea to the solvent-induced crystallization phenomenon of sPS.

Experimental Section

Samples. sPS powder (M_w 272 000, M_w/M_n 2.28) was kindly supplied by Idemitsu Petrochemical Co., Ltd. The glassy samples were prepared by quenching the molten films into ice water. Check of the amorphous content was made by measuring the FT-IR spectra at room temperature. The thickness of the samples was about 50 μm for the time-resolved IR measurements and about 100 μm for Raman and X-ray measurements. aPS films were prepared by melting the films cast from the chloroform solution.

Measurements. In the time-resolved measurements of infrared spectra for the samples subjected to the solvent atmosphere, the homemade cell was used, the size of which was about 4 cm (height) × 2 cm (width) × 1.5 cm (path length). The measurement was started at the same time with the solvent injection, and the data were saved at a constant time interval. Strictly speaking, we need to take into consideration the diffusion rate of solvent vapor; i.e., the solvent might take some time to reach the sample position and penetrate into the sample. But, in this experiment, the solvent vapor was assumed in a good approximation to fill the small sample cell quite rapidly after the solvent injection. Therefore, the solvent injection time was set equal to the starting time of the measurements. The infrared spectra were taken at a resolution power 2 cm^{-1} at a time interval of 16 s by using a Bio-Rad FTS-60A FT-IR spectrometer equipped with an MCT (mercury−cadmium−telluride) semiconductor detector. The solvents used were chloroform, benzene, and toluene. When the sample was exposed to a solvent, the sample was expanded more or less and the sample thickness changed. But this effect on the change in the infrared absorbance was checked to be small from the measurement of the thickness before and after experiment. The temperature dependence of the infrared spectra of aPS was measured at a constant time interval in the heating process from room temperature to 150 °C at the heating rate of 2 °C/min.

Results and Discussion

IR Bandwidth and Molecular Motion of aPS. To check an intimate relation between the molecular motion of the amorphous chain and the infrared bandwidth, the infrared spectral change of aPS was measured in the heating process from room temperature as shown in Figure 1. It may be needed to notice that an ideal check of the molecular motion half-width relationship for the amorphous chains is to do the experiment in which the aPS is exposed to the same kind of solvent with that used in the sPS experiment and to observe the change in the half-width of the amorphous band. But we do not have any clear information about the solvent-induced enhancement of molecular motion of the aPS chains. Rather, the motional activation by heating above the glass transition temperature is considered to be more direct to check the above-mentioned mobility

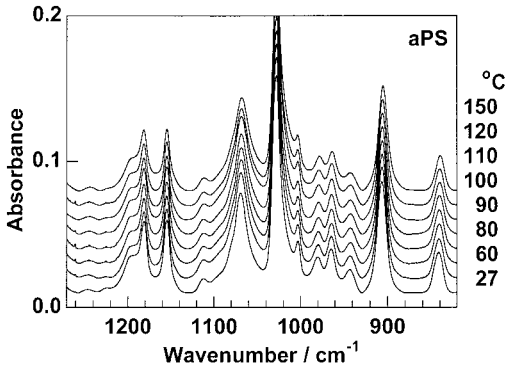

Figure 1. Infrared spectral change of atactic polystyrene measured in the heating process from room temperature.

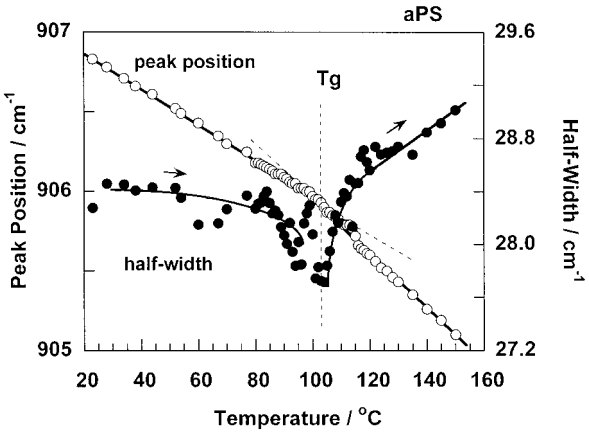

Figure 2. Temperature dependence of half-width and vibrational frequency of the amorphous infrared band of aPS sample at 907 cm^{-1}.

half-width relationship in the amorphous chains. Figure 2 shows the peak position and half-width of the 907 cm^{-1} amorphous band of aPS as a function of temperature. In the temperature region below T_g the half-width was almost constant, but it increased steeply above T_g. At the same time, with increasing temperature, the peak position of the band shifted to lower frequency side with a deflection point around T_g. The similar change could be seen also for the other bands. Therefore, we may say that the half-width and the peak position can become a good measure to indicate the enhancement of molecular motion in the amorphous region. (In Figure 2 the half-width was observed apparently to show a minimum in the vicinity of T_g, just like a slowing down phenomenon observed as the critical phenomenon in the phase transition of ferroelectric materials.[9] But it is not clear to assign the apparent minimum in the half-width to such a critical phenomenon occurring cooperatively in the amorphous region.)

This technique was actually applied to the solvent-induced crystallization phenomenon of sPS sample. Figure 3 shows, as an example, the infrared spectral change of sPS glass sample exposed to toluene atmosphere at room temperature. The amorphous bands are observed in the frequency region of 500−600 cm^{-1}. The spectral profile was separated into several components by using the software WIN-IR, and the peak position, half-width, and integrated intensity of each component were evaluated. The time dependence of the half-width, peak frequency, and integrated intensity of the band component at 568 cm^{-1} is shown in Figure 4. A similar plot is made also for the case of benzene as shown in Figure 5. In these figures the time evolution of the

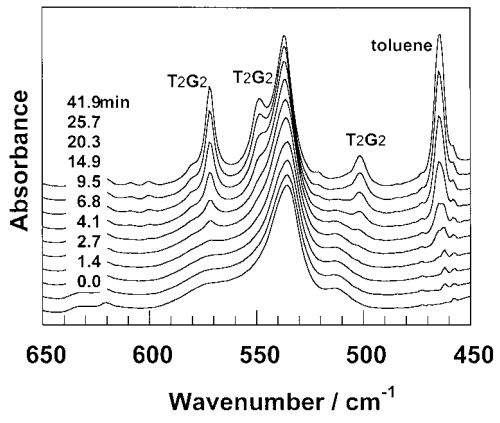

Figure 3. Infrared spectral change of the sPS glass sample exposed to toluene atmosphere at room temperature.

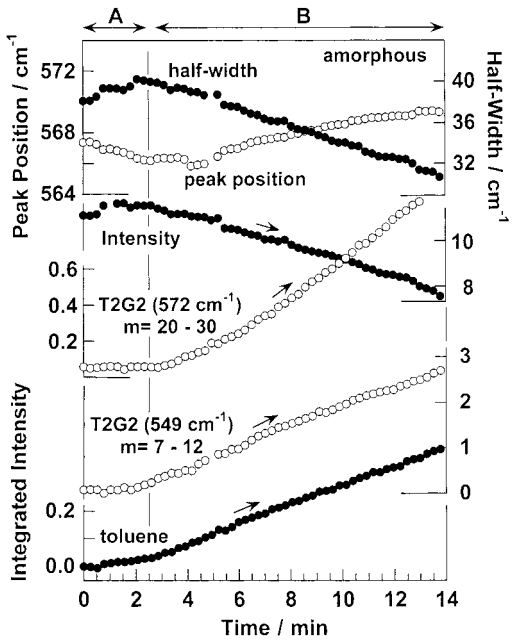

Figure 4. Time dependence of the half-width, peak frequency, and integrated intensity evaluated for the 568 cm^{-1} amorphous band in comparison with the intensity change of the crystalline bands (572 and 549 cm^{-1}) of sPS sample exposed to toluene vapor. In region A, the half-width of the amorphous band increased and the peak position shifted to lower frequency side as the toluene band increased in intensity. In this time region there occurred no crystallization as seen from the flat curves of the crystalline bands. In region B the crystallization started, and the crystalline bands increased in intensity. The band at 549 cm^{-1} with shorter critical sequence length m increased in intensity at first, and then the 572 cm^{-1} band with longer m value increased the intensity. Correspondingly, the amorphous band decreased the half-width and shifted toward the higher frequency side due to the constraint from the generated crystalline lamellae surrounding the amorphous chains.

integrated intensity of the crystalline bands is also shown. As already discussed in detail in the previous paper,[7] the values of critical sequence length m are given for these crystalline bands: the infrared band can be detected for the first time when the length of regular helical segment is beyond m.[10,11] Figures 4 and 5 may be divided into two time regions.

Time Region A. Immediately after the injection of solvent into the glassy sPS film, the intensity of solvent bands started to increase, and at the same time the half-width of the amorphous band at 568 cm^{-1} began to increase. The peak position of this band was found to

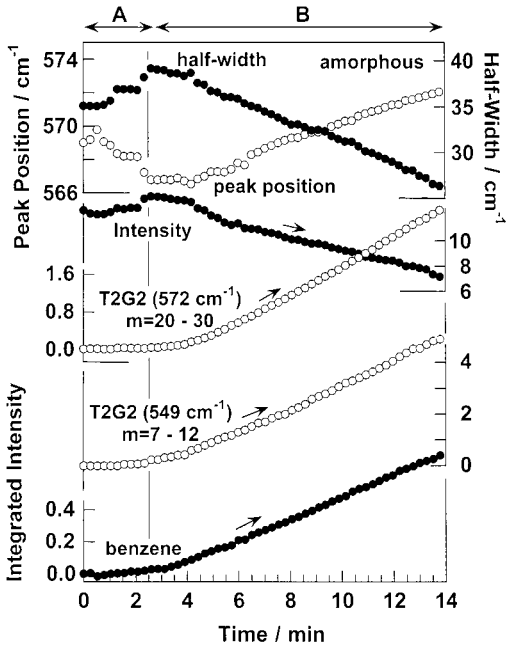

Figure 5. Time dependence of the half-width, peak frequency, and integrated intensity evaluated for the 568 cm^{-1} amorphous band in comparison with that of the intensity change of the crystalline bands of sPS sample exposed to benzene vapor. Each infrared band is found to behave in the same way with that explained in Figure 4.

shift to lower frequency side. These phenomena may be interpreted in terms of the enhancement of the molecular motion in the amorphous region. A slight increase in intensity of the amorphous band might be caused by dissolution of the locally regular domain in the glassy state into more irregular structure.

Time Region B. Around 2 min after the solvent injection (the case of toluene), the half-width of the amorphous band started to decrease, and the corresponding peak position shifted to higher frequency side. The intensity decreased largely with time. In parallel to these phenomena, the crystalline bands with short m ($m = 7-12$ monomeric units for the band at 549 cm^{-1}) started to increase their intensities. The intensity of the crystalline bands with long m ($m = 20-30$ for the band at 572 cm^{-1}) increased a little later than the bands with shorter m.

From these experimental data the following scheme may be deduced for the two time regions. After the injection of solvent, the amorphous chain interacts with the solvent and accelerates the mobility even below T_g, as seen in the change of half-width and peak position of the amorphous bands in the time region A. This chain motion plays as a trigger to cause the conformational ordering to generate the short helical segments in the time region B. Once these short helices are created, they work as a nucleus and longer helical segments are grown, as seen in Figure 6a−c. When the crystallization started to progress in this way, the half-width of the amorphous bands began to decrease, and the peak position shifted toward higher frequency side. These phenomena are considered to come from the reduction of the mobility of the amorphous chains which are constrained more or less in between the developed crystalline parts.

In parallel to these infrared spectral measurements, the time-resolved X-ray diffraction measurement was made in the course of solvent-induced crystallization.

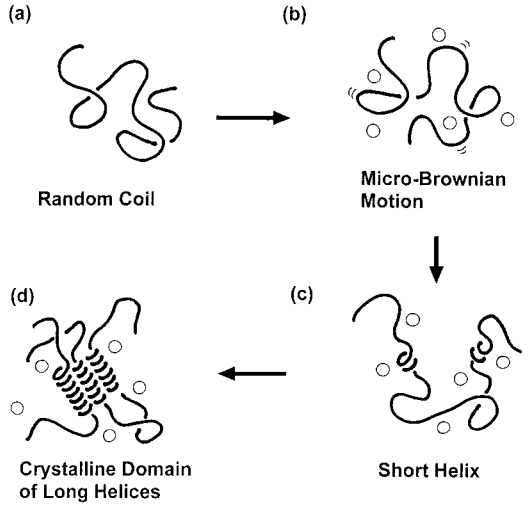

Figure 6. Schematic illustration of structural change in the process of solvent-induced crystallization of sPS. Random coil in the amorphous part (a) is activated to make a micro-Brownian motion (b) by absorbing solvent molecules, and then the short regular helical segments are generated (c), which grow to longer helices and form the crystalline lattice (d).

As already reported,[7] the intensity change of the crystalline peaks or the relative crystallinity was evaluated and compared with the infrared and Raman spectral data. It was found that the crystallinity evaluated from the X-ray diffraction intensity started to increase in the time region of appearance of helical bands with long critical sequence length. This indicates the formation of a crystalline lattice, having a finite size detectable by a coherent X-ray diffraction, can be realized for the first time when the long helical segments are formed in the glassy sample. A concrete image is shown in Figure 6d. In this way, by combining the various kinds of experimental data of infrared, Raman, and X-ray diffraction, we could deduce quite concretely the structural evolution from the amorphous phase of random coils to the crystalline lattice of regular helices through an occurrence of micro-Brownian motion of the chains by absorption of organic solvent.

Effect of Solvent Species on Crystallization Process. Using the samples of the same film thickness, a similar measurement was made for the various types of solvent: chloroform, benzene, and toluene. Figure 7 shows the time evolution of the crystalline fraction evaluated from the infrared spectra. The T_2G_2 helical bands begin to appear after some induction time, the length of which depends remarkably on the kind of the solvent. The induction period is in the order of chloroform < benzene < toluene. The slope of the curve or the crystallization rate is also different: chloroform ≫ benzene > toluene. A similar tendency is observed also for the occurrence of micro-Brownian motion of the amorphous chains. Figure 8a−c shows the time dependence of the half-width and peak position of the infrared amorphous band measured for the sPS glasses exposed to chloroform, benzene, and toluene, respectively. As mentioned above, the time to reach the maximum in the half-width and the minimum in the vibrational frequency correspond to the starting time of the formation of regular T_2G_2 helical segments. The induction period observed in Figure 7 is a little longer than the time showing the maximum in the half-width and minimum in the peak frequency for all these cases, indicating that the induction period consists, at least,

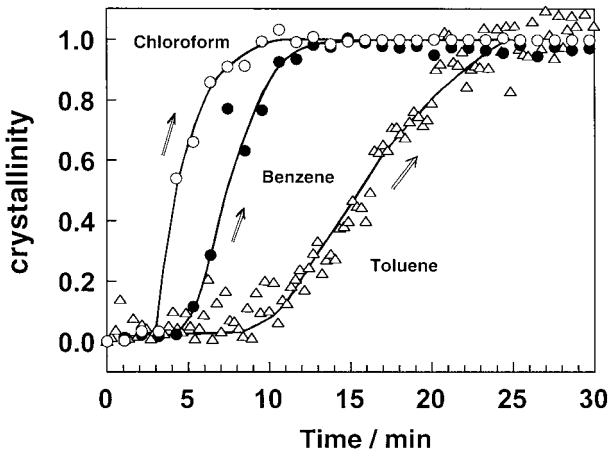

Figure 7. Comparison of the time dependence of the infrared intensity of the crystalline bands estimated for the sPS glass samples subjected to the various kinds of solvent atmosphere (room temperature).

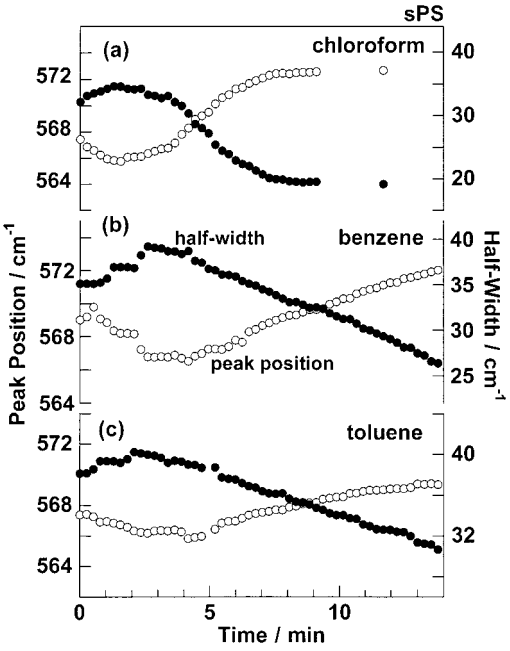

Figure 8. Time dependence of the half-width and peak position of the amorphous band measured for the sPS glass sample exposed to (a) chloroform, (b) benzene, and (c) toluene.

of the time of diffusion of solvent molecules into the amorphous chain matrix and the starting of the micro-Brownian motion of the amorphous chains. Chloroform induces the molecular motion of the amorphous chains quite rapidly compared with the cases of benzene and toluene. In the case of toluene, the motion occurs gradually in a wider time range. Chloroform molecules interact strongly with the sPS chains and activate the molecular motion of the chains in relatively short time, which can be speculated reasonably from the experimental fact that chloroform is a good solvent for sPS, as discussed in the previous paper.[7] The inversed tendency is seen for the case of toluene, which is a poor solvent for sPS, and the activation of molecular motion and the formation of the regular helix occur in a relatively slow timing.

For the discussion of the diffusion process of solvent molecules in the sample[12−16] and the mechanism how the solvent molecules interact with the chains[17−21] and cause the chain motion, we need to study the crystal-

lization phenomenon in more detail at higher time resolution.

Conclusion

In the present paper we have shown the infrared spectral data to confirm the prediction that the amorphous sPS chains must be activated by solvent molecules before the crystallization phenomenon occurs even at room temperature much lower than T_g. By combining all the experimental data of infrared, Raman, and X-ray diffraction collected during the solvent-induced crystallization phenomenon of sPS glassy sample, a plausible scheme has been obtained to describe the detailed and concrete structural evolution of the random coil into the regular helical chain and the formation of crystalline lattice constructed by a packing of these regular helical segments. Interaction between random coil and organic solvent induces the micro-Brownian motion of the amorphous chain, which accelerates the regularization of the random coil into a helical conformation. The thus created short helical segments grow longer and gather together to generate the crystalline domains. The difference in strength of interaction between polymer and solvent is dependent on the type of the solvent. The chloroform interacts more strongly with sPS chain, while toluene interacts with sPS chain relatively mildly, reflecting on slower and broader activation of molecular motion, longer induction period, and slower crystallization rate.

It might be a natural image for the amorphous chain to start to activate in the course of crystallization through the interaction with the injected solvent molecules. But we wish to emphasize here that such information on molecular motion followed by regularization to helical segments could be obtained for the first time when many kinds of experimental data including infrared, Raman, and X-ray diffraction were collected and interpreted systematically and consistently.

Acknowledgment. The authors thank Idemitsu Petrochemical Co., Ltd., Japan, for supplying sPS samples.

References and Notes

(1) (a) Ishihara, N.; Seimiya, T.; Kuramoto, M.; Uoi, M. *Macromolecules* **1986**, *19*, 2465. (b) Kobayashi, M.; Nakaoki, T.; Ishihara, N. *Macromolecules* **1989**, *22*, 4377. (c) Reynolds, N. M.; Savage, J. D.; Hsu, S. L. *Macromolecules* **1989**, *22*, 2869. (d) Greis, O.; Xu, Y.; Petermann, J. *Polymer* **1989**, *30*, 590. (e) Zimba, C. G.; Rabolt, J. F. *Macromolecules* **1989**, *22*, 2867. (f) Guerra, G.; Vincenzo, V.; Vitagliano, M.; De Rosa, C.; Petraccone, V.; Corradini, P. *Macromolecules* **1990**, *23*, 1539. (g) Kobayashi, M.; Nakaoki, T.; Ishihara, N. *Macromolecules* **1990**, *23*, 78. (h) Reynolds, N. M.; Hsu, S. L. *Macromolecules* **1990**, *23*, 3463. (i) Gomez, M. A.; Tonelli, A. E. *Macromolecules* **1990**, *23*, 3385. (j) Nakaoki, T.; Kobayashi, M. *J. Mol. Struct.* **1991**, *242*, 315. (k) Chatani, Y.; Shimane, Y.; Inoue, Y.; Inagaki, T.; Ijitsu, T.; Yukinari, T. *Polymer* **1992**, *33*, 488. (l) Nyquist, R.; Putzig, C. L.; Leugers, M. A.; McLachlan, R. D.; Thill, B. *Appl. Spectrosc.* **1992**, *46*, 981. (m) Savage, J. D.; Wang, Y. K.; Stidham, H. D.; Corbett, M.; Hsu, S. L. *Macromolecules* **1992**, *25*, 3164. (n) Vittoria, V.; Russo, R.; de Candia, F.; Carotenuto, M.; Guadaguno, L. *J. Macromol. Sci., Phys.* **1996**, *B35*, 265. (o) Lawrence, S.; Shinozaki, D. M. *Polym. Eng. Sci.* **1997**, *37*, 1825. (p) Musto, P.; Tavone, S.; Guerra, G.; de Rosa, C. *J. Polym. Sci., Part B: Polym. Phys.* **1997**, *35*, 1055. (q) Xue, Y. L. *Macromol. Rapid Commun.* **1998**, *19*, 549. (r) Berghmans, H.; De Cooman, R.; De Rudder, J.; Koningsveld, R. *Polymer* **1998**, *39*, 4621. (s) Berghmans, H.; Aerts, L.; Buyse, K.; Deberdt, F.; Roels, T.; De Rudder, J.; Vereecke, S. Ber. *Bunsen-Ges. Phys. Chem.* **1998**, *102*, 1654. (t) Woo, E. M.; Sun, Y. S.; Lee, M. L. *Polymer* **1999**, *40*, 4425. (u) Brulet, A.; Boue, F.; Menelle, A.; Cotton, J. P. *Macromolecules* **2000**, *33*, 997.

(2) (a) Greis, O.; Xu, Y.; Asano, T.; Petermann, J. *Polymer* **1989**, *30*, 590. (b) Pradere, P.; Thomas, E. L. *Macromolecules* **1990**, *23*, 4954. (c) de Candia, F.; Romano, G.; Russo, R.; Vittoria, V. *Colloid Polym. Sci.* **1990**, *268*, 720. (d) De Rosa, C.; Guerra, G.; Petraccone, V.; Corradini, P. *Polym. J.* **1991**, *23*, 1435. (e) De Rosa, C.; Rapacciulo, M.; Guerra, G.; Petraccone, V.; Corradini, P. *Polymer* **1992**, *33*, 1423. (f) Chatani, Y.; Shimane, Y.; Ijitsu, T.; Yukinari, T. *Polymer* **1993**, *34*, 1625. (g) Sun, Z.; Millar, R. L. *Polymer* **1993**, *34*, 1963. (h) Corradini, P.; De Rosa, C.; Guerra, G.; Napolitano, R.; Petraccone, V.; Porozzi, B. *Eur. Polym. J.* **1994**, *30*, 1173. (i) Kestenbach, H. J.; Petermann, J. *Acta Polym.* **1994**, *45*, 294. (j) De Rosa, C. *Macromolecules* **1996**, *29*, 8460. (k) Tosaka, M.; Hamada, N.; Tsuji, M.; Kohjiya, S.; Ogawa, T.; Isoda, S.; Kobayashi, T. *Macromolecules* **1997**, *30*, 4132. (l) Hamada, N.; Tosaka, M.; Tsuji, M.; Kohjiya, S.; Katayama, K. *Macromolesules* **1997**, *30*, 6888. (m) Tosaka, M.; Hamada, N.; Tsuji, M.; Kohjiya, S. *Macromolecules* **1997**, *30*, 6592.

(3) (a) Cartier, L.; Okihara, T.; Lotz, B. *Macromolecules* **1998**, *31*, 3303. (b) Tosaka, M.; Tsuji, M.; Kohjiya, S.; Cartier, L.; Lotz, B. *Macromolecules* **1999**, *32*, 4905. (c) Vittoria, V.; Filho, A. R.; de Candia, F. *Polym. Bull.* **1991**, *26*, 445. (d) Chatani, Y.; Shimane, Y.; Inagaki, T.; Ijitsu, T.; Yukinari, T.; Shikuma, H. *Polymer* **1993**, *34*, 1620. (e) Chatani, Y.; Inagaki, T.; Shimane, Y.; Shikuma, H. *Polymer* **1993**, *34*, 4841. (f) de Candia, F.; Carotenuto, M.; Guadagno, L.; Vittoria, V. *J. Macromol. Sci., Phys.* **1996**, *B35*, 265. (g) Spells, S. J. *Macromol. Symp.* **1997**, *114*, 63. (h) Tsutsui, K.; Tsujita, Y.; Yoshimizu, H.; Kinoshita, T. *Polymer* **1998**, *39*, 5177. (i) Moyses, S.; Sonntag, P.; Spells, S. J.; Laveix, O. *Polymer* **1998**, *39*, 3537. (j) Tsutsui, K.; Katsumata, T.; Fukatsu, H.; Yoshimizu, H.; Kinoshita, T.; Tsujita, Y. *Polym. J.* **1999**, *31*, 268. (k) Tsutsui, K.; Katsumata, T.; Yamamoto, Y.; Fukatsu, H.; Yoshimizu, H.; Kinoshita, T.; Tsujita, Y. *Polymer* **1999**, *40*, 3815. (l) de Rosa, C.; Rizzo, P.; de Ballesteros, O. R.; Petraccone, V.; Guerra, G. *Polymer* **1999**, *40*, 2103.

(4) (a) Reynolds, N. M.; Stidham, H. D.; Hsu, S. L. *Macromolecules* **1991**, *24*, 3662. (b) Wang, Y. K.; Savage, J. D.; Yang, D.; Hsu, S. L. *Macromolecules* **1992**, *25*, 3659. (c) De Rosa, C.; Guerra, G.; Petraccone, V.; Pirozzi, B. *Macromolecules* **1997**, *30*, 4147. (d) Roels, T.; Rastogi, S.; De Rudder, J.; Berghmans, H. *Macromlecules* **1997**, *30*, 7939. (e) Rastogi, S.; Goossens, J. G. P.; Lemstra, P. J. *Macromolecules* **1998**, *31*, 2983. (f) Guatagno, L.; Baldi, P.; Vittoria, V.; Guerra, G. *Macroomol. Chem. Phys.* **1998**, *199*, 2671. (g) Goossens, H.; Rastogi, S.; Lemstra, P. *Macromol. Symp.* **1999**, *138*, 99. (h) De Rudder, J.; Berghmans, H.; Arnautss, J. *Polymer* **1999**, *40*, 5919. (i) Naddeo, C.; Guadagno, L.; Acierno, D.; Vittoria, V. *Macromol. Symp.* **1999**, *138*, 209. (j) Moyses, S.; Spells, S. J. *Macromolecules* **1999**, *32*, 2684. (k) Zhu, C. S.; Dou, H. J.; He, S. Q.; Mo, Z. S. Chin. *Chem. Lett.* **2000**, *11*, 93.

(5) Tashiro, K.; Ueno, Y.; Yoshioka, A.; Kaneko, F.; Kobayashi, M. *Macromol. Symp.* **1999**, *141*, 33.

(6) Tashiro, K.; Sasaki, S.; Ueno, Y.; Yoshioka, A.; Kobayashi, M. *Korea Polym. J.* **2000**, *8*, 103.

(7) Tashiro, K.; Ueno, Y.; Yoshioka, A.; Kobayashi, M. *Macromolecules* **2001**, *34*, 310.

(8) Fröhlich, H. *Theory of Dielectrics*, 2nd version; Oxford: London, 1960.

(9) Hatta, I. *J. Phys. Soc. Jpn.* **1968**, *24*, 1043.

(10) Kobayashi, M.; Akita, K.; Tadokoro, H. *Makromol. Chem.* **1968**, *118*, 324.

(11) Kobayashi, M. *Macromol. Symp.* **1997**, *114*, 1.

(12) Roels, T.; Deberdt, F.; Berghmans, H. *Macromolecules* **1994**, *27*, 6216.

(13) Daniel, C.; Menelle, A.; Brulet, A.; Guenet, J. M. *Macromol. Symp.* **1997**, *114*, 159.

(14) Guenet, J. M. *Macromol. Symp.* **1997**, *14*, 1197.

(15) Guerra, G.; Manferedi, C.; Musto, P.; Tavone, S. *Macromolecules* **1998**, *31*, 1329.

(16) Musto, P.; Manzari, M.; Guerra, G. *Macromolecules* **2000**, *33*, 143.

(17) Vittoria, V.; Russo, R.; de Candia, F. *Makromol. Chem., Macromol. Symp.* **1990**, *39*, 317.

(18) Vittoria, V.; Russo, R.; de Candia, F. *Polymer* **1991**, *32*, 3371.

(19) Kobayashi, M.; Kozasa, T. *Appl. Spectrosc.* **1993**, *47*, 1417.

(20) Daniel, C.; Menelle, A.; Brulet, A.; Guenet, J. M. *Polymer* **1997**, *38*, 4193.

(21) Daniel, C.; Deluca, M. D.; Guenet, J. M.; Brulet, A.; Menelle, A. *Polymer* **1996**, *37*, 1273.

MA011509X